NANO LETTERS

2007
Vol. 7, No. 5
1186−1190

Effects of Quantum Confinement on the Doping Limit of Semiconductor Nanowires

D. R. Khanal,[†,‡] Joanne W. L. Yim,[†,‡] W. Walukiewicz,[‡] and J. Wu*[,†,‡]

Department of Materials Science and Engineering, University of California, Berkeley, Berkeley, California 94720, and Materials Sciences Division, Lawrence Berkeley National Laboratory, Berkeley, California 94720

Received December 8, 2006; Revised Manuscript Received February 23, 2007

ABSTRACT

We have calculated the effects of quantum confinement on maximum achievable free carrier concentrations in semiconductor nanowires. Our calculations are based on the amphoteric defect model, which describes the thermodynamic doping limit in semiconductors in terms of the compensation of external dopants by native defects. We find that the generation of amphoteric native defects strongly limits maximum achievable carrier concentrations for nanowires with small widths where quantum confinement is appreciable. The magnitude of this effect in a given material is found to be determined by two material properties: the effective mass of the free carriers, and the position of the conduction (n-type) or valence band (p-type) edge on the absolute energy scale. These results offer a simple, predictive guideline for designing nanostructure devices and contacts where high doping levels are needed.

Semiconductors with electron confinement offer a distinct way to study electrical and thermal transport phenomena as a function of dimensionality and size reduction. Quasi-one-dimensional (1D) semiconductors are also promising candidates for integration of novel electronic[1,2] and photonic[3] circuits. The wide range of demonstrated and potential applications has made semiconductor nanowires a growing focus of research in recent years. Successful realization of some of these applications requires high carrier concentrations to allow for sufficient conductivity and/or Fermi level displacement. Unfortunately, many semiconductors are notoriously difficult to dope even in bulk form.[4] For example, reliable and well-controlled p-type doping of ZnO and InN has not been experimentally demonstrated. Using local density approximation calculations, it has been theoretically predicted that in GaAs quantum dots, the quantum confinement effect tends to stabilize the deep defect, the DX center, and consequently makes extrinsic doping less effective than in the bulk.[5] This is corroborated experimentally with a lack of reported high doping levels in semiconductor nanostructures. It is, therefore, of great importance to understand and predict the n- and p-type doping limits of semiconductor nanostructures in terms of their fundamental material parameters.

Doping limits in various bulk semiconductors are well explained by the amphoteric nature of compensating native defects. The amphoteric defect model (ADM)[4,6] considers the fact that the formation energy of charged native defects, such as vacancies and antisites, depends linearly on the Fermi level (E_F) in the crystal. In heavily damaged materials with high defect concentrations, it was discovered that the Fermi level always evolves toward the same energy value, known as the Fermi stabilization energy (E_{FS}).[4] In all materials, including those without high defect concentrations, the farther E_F moves away from E_{FS} by extrinsic doping, the lower the energy barrier is for the system to generate native defects that act to compensate the extrinsic dopants. That is, native defects are generated in semiconductor materials in response to extrinsic doping so as to pull E_F back toward E_{FS}. Depending on whether E_F is above or below E_{FS}, acceptor- or donor-like native defects are predominant, giving these defects their amphoteric character. The net effect is that it is increasingly difficult to move E_F away from E_{FS} by adding external dopants, as the dopants will be more easily compensated by native defects. In equilibrium conditions, after significant external doping, E_F eventually saturates at a limit value ($E_{F-\mathrm{limit}}$) away from E_{FS}. At this point, the formation energy for native defects is sufficiently low so that any additional dopants will be fully compensated. This imposes an effective, thermodynamic limit to E_F and hence the free carrier concentrations.

The Fermi stabilization level, also termed the branch point energy[7] or the charge neutrality level, has been shown to have a universal energy of about 4.9 eV below the vacuum level,[4] independent of the chemical identities of the host

* To whom correspondence should be addressed. E-mail: wuj@berkeley.edu.
† Department of Materials Science and Engineering, University of California, Berkeley.
‡ Materials Sciences Division, Lawrence Berkeley National Laboratory.

10.1021/nl062886w CCC: $37.00 © 2007 American Chemical Society
Published on Web 03/28/2007

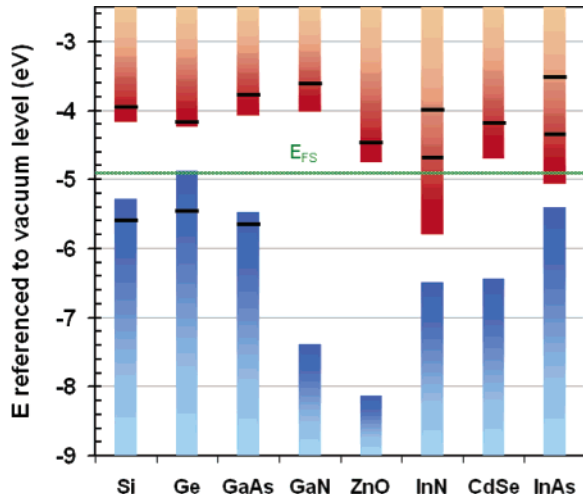

Figure 1. Band offsets and E_{FS} for the eight semiconductors studied. Red and blue bins represent the conduction and valence bands, respectively. Black bars within bands represent $E_{F-limit}$ in bulk obtained from literature values of maximum carrier concentrations for electrons and holes. For n-InN and n-InAs, two bars were shown, corresponding to calculated $E_{F-limit}$ using parabolic (upper bar) and nonparabolic (lower bar) conduction band dispersion, respectively. Reported electron concentrations for Si, Ge, GaAs, GaN, ZnO, InN, CdSe, and InAs were obtained from refs 11, 13, 15, 17, 18, 19, 20, and 21, respectively. Reported hole concentrations for Si, Ge, and GaAs were obtained from refs 12, 14, and 16, respectively.

material or dopant species. This is due to the fact that the amphoteric native defects are strongly localized in real space, similar to the universally aligned transition metal defect levels.[8,9] Their wavefunctions in k-space thus sample the entire Brillouin zone, leading to an energy level that is determined by regions with a large density of states, and is insensitive to the band edges of the host, which have a small density of states. This universal alignment of E_{FS} is shown in Figure 1, together with the natural band edge offsets of various semiconductors investigated in this study.[4] The strong doping disparity in these semiconductors is explained by the large asymmetry of their conduction band edge (E_C) and valence band edge (E_V) with respect to E_{FS}. For example, p-type doping is difficult in GaN, ZnO, and InN because their E_V is far below E_{FS}, while InAs and InN[10] have a strong propensity toward n-type character because E_{FS} is located above their E_C instead of in their band gap. Also shown in Figure 1 are the positions of $E_{F-limit}$ back-calculated using maximum reported electron or hole concentrations in bulk materials grown by equilibrium methods.[11−21] In n-type InAs and InN, $E_{F-limit}$ is located deep into the conduction band such that the strongly nonparabolic part of the conduction band is populated.[19] In Figure 1, we show the range of $E_{F-limit}$ back-calculated for n-type InN and InAs, where the lower bar corresponds to $E_{F-limit}$ for the nonparabolic conduction band, and the upper bar is $E_{F-limit}$ when the band is approximated by a parabolic dispersion with electron effective mass equal to the mass at E_C.

Upon hydrostatic pressure or isoelectronic alloying, shallow dopant levels closely follow the movement of E_C (for donors) or E_V (for acceptors). In contrast, the energy of strongly localized defects remains relatively constant under these external stimuli.[22] The insensitivity to local band extrema of transition metal impurity levels has been used to determine the band offsets in III−V and II−VI compounds[9] and the band edge deformation potentials in GaAs and InP.[23] These distinctly different sensitivities of shallow and localized defect levels also hold true in the case of quantum confinement.[5] When size is reduced in semiconductor nanostructures, the density of states (DOS) is restructured and the energies of allowed states shift upward from the original E_C (for n-type) or downward from E_V (for p-type); however, the Fermi stabilization energy and the Fermi level limits *remain unchanged* due to their origination from strongly localized defects with a spatial extension (<a few atoms) much smaller than the spatial confinement of the system.[5] Consequently, the maximum achievable carrier concentration is suppressed with size reduction. In this paper, we calculate the effect of quantum confinement on the doping limit of semiconductor nanowires in the context of the ADM, taking into account the relatively constant positions of E_{FS} and $E_{F-limit}$ with quantum confinement. We assume a full passivation of surface states, such that surface Fermi level pinning is absent and E_F is constant throughout the nanowire.[24]

Free carriers in nanowires are confined in the cross-sectional dimensions (x and y), allowing only one free dimension (z) and making nanowires a quasi-1D system. We model this confinement using envelope wavefunctions in the framework of the effective mass theory.[22] Ignoring the facet difference of various semiconductor nanowires, the confinement in the (x,y) plane is approximated by an infinitely deep square well with width a. The 1D density of states (per volume) for a single valley in the band structure is the sum over multiple confinement subbands

$$\rho^{1D}(E) = \frac{1}{\pi\hbar a^2}\sum_{N_x,N_y}\sqrt{\frac{2m_z^*}{E-(E_0+E_{N_xN_y})}} \qquad (1)$$

where E_0 is E_C (for n-type) or E_V (for p-type), and m_z^* is the effective mass of carriers along the nanowire length direction. $E_{N_xN_y} = \hbar^2\pi^2(N_x^2 + N_y^2)/2m_{xy}^*a^2$ is the quantized energy level, and m_{xy}^* is the effective mass in (x,y) plane, which can be different from m_z^* (for n-type indirect band gap semiconductors such as Si and Ge). The quantization of the energy in (x,y) plane gives rise to van Hove singularities in the DOS corresponding to the onset of sequential confinement levels. In Figure 2, the DOS is plotted for GaAs with two different nanowire widths and compared to the standard 3D DOS. As the nanowire dimensions increase to over ~50 nm, the 1D DOS begins to merge with the 3D DOS as expected.

The maximum achievable carrier concentration is obtained by integrating the 1D DOS shown in eq 1 from $E = E_0$ to $E_{F-limit}$. The sum in eq 1 runs from $(N_x,N_y) = (1,1)$ to the subband of (N_x,N_y) given by $E_0 + E_{N_xN_y} \leq E_{F-limit}$. As all the materials investigated have $E_{F-limit}$ far from E_0 (much more

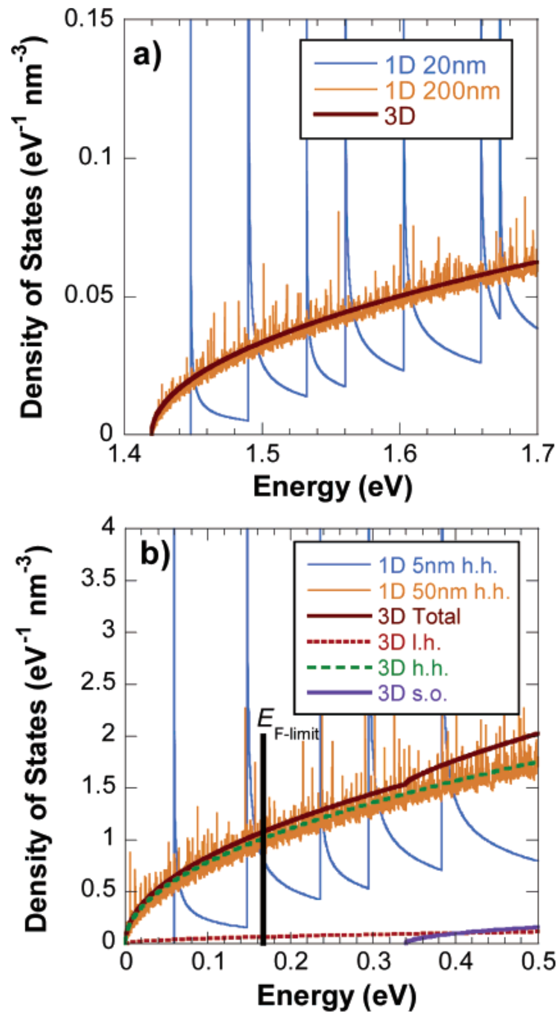

Figure 2. (a) One-dimensional conduction band DOS for GaAs nanowires of widths 20 and 200 nm plotted from the conduction band edge to $E_{F-limit}$ (1.705 eV). Three-dimensional DOS is also shown. (b) One-dimensional valence band DOS for nanowires of widths 5 and 50 nm compared to 3D DOS. $E_{F-limit}$ (0.167 eV) is shown. Density of states from heavy-hole, light-hole, and split-off bands are separately shown for 3D. The total valence band DOS is dominated by the heavy-hole band.

than $k_BT = 26$ meV away), the temperature broadening was safely neglected in the total carrier concentration calculation. For tetrahedrally structured semiconductors, the valence band DOS is a sum of the DOS from heavy-hole, light-hole, and split-off bands with distinct effective masses. As shown in Figure 2b, the total valence band DOS for the 3D case is dominated by the heavy-hole band, which has the greatest effective mass. Also, for n-type indirect-band gap Si and Ge, multiple conduction band valleys were taken into account by including a multiplicative degeneracy factor in eq 1.

Figure 3 shows the dependence of maximum achievable carrier concentration (n_{lim} or p_{lim}) on the nanowire width for the semiconductors investigated. This maximum achievable carrier concentration is strongly suppressed when the nanowire width is below ~20 nm, typical of semiconductor nanowires grown by the vapor−liquid−solid approach. There is an onset width below which the carrier concentration is zero. This onset corresponds to the width where the ground level (E_{11}) is raised beyond $E_{F-limit}$ by the quantum confinement. The fine features in the curves at very small widths reflect single subbands moving across $E_{F-limit}$ and causing sharp rises in the total carrier concentration. At large nanowire widths, the maximum achievable carrier concentrations quickly approach bulk values. It should be noted, however, that parts a and b of Figure 3 are plots of theoretical limits to carrier concentrations calculated in this model. Experimentally reported carrier concentrations can be substantially lower than these limits for mainly two reasons. First, during growth, most nanowires are not intentionally doped up to their maximum limit. Second, this model assumes complete passivation of surface states so as for E_F to be displaced solely by doping. When this condition is not fulfilled, E_F can be pinned by surface states, resulting in additional doping inefficiency. We performed a survey of reported carrier concentrations in nanowires, and the obtained values are all within the limits shown in Figure 3. These include, for example, $n = 10^{18}-10^{19}$ cm^{-3} in GaN with a diameter of 67 nm reported by Huang et al.,[25] $n = 2 \times 10^{17}$ cm^{-3} in InAs with a diameter of 80 nm reported by Bryllert et al.,[26] $n = 7 \times 10^{17}$ cm^{-3} in ZnO with a diameter of 42.5 nm reported by Yun et al.,[27] and $p = 10^{18}$ cm^{-3} in Si with a diameter of 15 nm reported by Cui et al.[28]

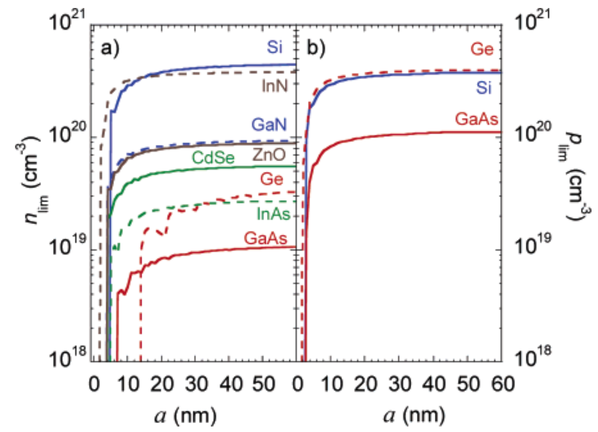

Figure 3. Maximum achievable electron (a) and hole (b) concentrations in various semiconductor nanowires as a function of nanowire width a.

We note that the rate at which the carrier concentration limit is reduced is not the same for all semiconductors. A characteristic wire width (a_c) can be defined as the width at which the 1D carrier concentration limit equals half of the maximum bulk carrier concentration. It can be shown from eq 1 that the ratio of 1D to 3D doping limits is given by the following dimensionless expression,

$$\frac{n_{limit}^{1D}}{n_{limit}^{3D}} = \frac{6}{\pi}\xi \cdot \sum_{N_x,N_y}\sqrt{1-\xi\cdot(N_x^2+N_y^2)} \quad (2)$$

where $\xi = (\hbar^2\pi^2/2m_{xy}^*a^2)/|E_{F-limit} - E_0| \leq {}^1/_2$. Therefore, it is seen that the characteristic a_c that makes the ratio in eq 2 be 0.5 obeys a scaling law as

$$a_c \propto \frac{1}{\sqrt{m^*_{xy} \cdot |E_{F-limit} - E_0|}} \quad (3)$$

Figure 4 clearly shows this linear dependence for the various n- and p-type semiconductors, where a_c was numerically determined from the curves in Figure 3. In this plot, the nonparabolicity of the conduction band of InN and InAs is expected not to change a_c for *n*-InN and *n*-InAs, as the increase in m^*_{xy} will be fully compensated by the reduction of $|E_{F-limit} - E_0|$ in eq 3. In addition, for p-type semiconductors under strong quantum confinement, the heavy- and light-hole effective masses undergo a "mass reversal" as well as an overall change in their values.[22] Its effect on the total DOS (thus on p_{lim}) that includes both heavy- and light-hole bands, however, is relatively small (e.g., estimated to be <20% for GaAs). This is because the effect of a decrease in the heavy-hole mass is partially compensated by an increase in the light-hole mass.[22] We estimated the resultant maximum change in a_c from Figure 3 and indicated the range by vertical bars in Figure 4.

According to eq 3 and Figure 4, the size effect on maximum achievable doping concentrations is therefore determined by two *inherent* material properties, namely the effective masses of free carriers, and $E_{F-limit}$, measured from the conduction or valence band edges. The latter is loosely a function of the band edge position alone because of the relatively weak variation of the $E_{F-limit}$ position over different materials on the absolute energy scale (Figure 1). This picture can be used as a simple guide in estimating the size effect of doping limit in nanowires of various semiconductors and semiconductor alloys. For example, in n-type narrow band gap semiconductors such as InSb, a strong $k \cdot p$ interaction leads to a small electron effective mass ($<0.02m_0$); as a result, the suppression of doping limit should be readily seen at relatively large nanowire diameters. For p-type doping in the alloy $In_xGa_{1-x}N$, the heavy-hole effective mass does not change drastically from GaN ($\sim 1.3m_0$) to InN ($\sim 1.6m_0$), and $E_{F-limit}$ can be assumed to not vary as fast as the upward movement of E_V from GaN to InN; this implies an increasing $|E_{F-limit} - E_V|$ and thus a weaker size effect on the p-type doping limit with increasing x. Because the mechanism discussed here is not limited to the 1D geometry, a similar doping trend is expected in semiconductor nanostructures with different geometries such as quantum dots, tetrapods, core−shell structures, and ultrathin layers.

In summary, we have shown that quantum confinement in semiconductor nanowires decreases the maximum achievable doping concentration, effectively making nanowires more difficult to dope than their bulk counterparts. We have quantified these effects and shown that the effect of quantum confinement on the doping limit is an intrinsic material property that depends on the effective mass of free carriers and the band edge positions of the materials. Achieving high doping concentrations is essential for the realization of advanced nanowire applications such as devices where low-resistance contacts or tunnel junctions, narrow depletion widths, and modulation doping are needed. High carrier concentrations are also necessary in dilute magnetic semiconductors (DMSs), where the magnetism is mediated by free carriers. The suppression of maximum achievable carrier concentration in DMS nanostructures translates to a reduction in the Curie temperature expected in these nanostructures.

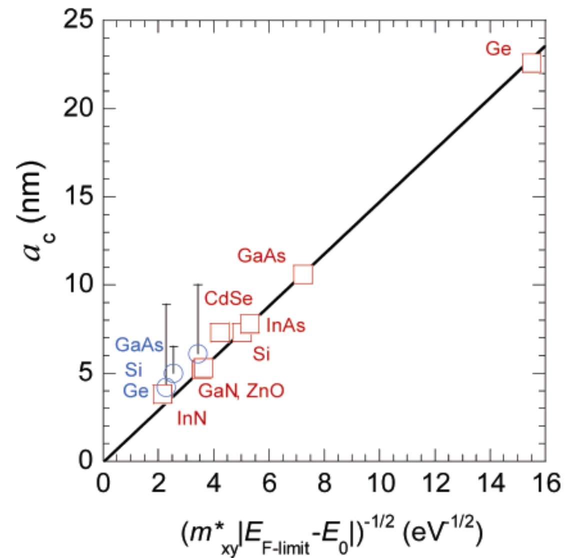

Figure 4. Characteristic nanowire width a_c for electron (squares) or hole (circles) doping as a function of conduction or valence band effective mass and relative Fermi level limit. Vertical bars indicate estimated range of a_c due to changes in hole effective mass caused by quantum confinement. Heavy-hole masses were used for valence band, and in-plane effective masses were used for the conduction band of indirect semiconductors. The straight line is a guide to the eye.

Acknowledgment. This paper is based upon work supported by the National Science Foundation under grant no. EEC-0425914. This work is also partially supported by the Director, Office of Science, Office of Basic Energy Sciences, Division of Materials Sciences and Engineering, of the U.S. Department of Energy under contract no. DE-AC03-76SF00098.

References

(1) Li, Y.; Qian, F.; Xiang, J.; Lieber, C. M. *Mater. Today* **2006**, *9*, 18.
(2) Lu, W.; Lieber, C. M. *J. Phys. D: Appl. Phys.* **2006**, *39*, R387.
(3) Sirbuly, D.; Law, M.; Yan, H.; Yang, P. *J. Phys. Chem. B* **2005**, *109*, 15191.
(4) Walukiewicz, W. *Physica B* **2001**, *302*, 123.
(5) Li, J. B.; Wei, S. H.; Wang, L. W. *Phys. Rev. Lett.* **2005**, *94*, 185501.
(6) Walukiewicz, W. *Appl. Phys. Lett.* **1989**, *54*, 2094.
(7) Tersoff, J. *Phys. Rev. B* **1985**, *32*, 6968.
(8) Caldas, M. J.; Fazzio, A.; Zunger, A. *Appl. Phys. Lett.* **1984**, *45*, 671.
(9) Langer, J. M.; Heinrich, H. *Phys. Rev. Lett.* **1985**, *55*, 1414.
(10) Mahboob, I.; Veal, T. D.; Piper, L. F. J.; McConville, C. F.; Lu, H.; Schaff, W. J.; Furthmueller, J.; Bechstedt, F. *Phys. Rev. B* **2004**, *69*, 201307.
(11) Balkanski, M.; Aziza, A.; Amzallag, E. *Phys. Status Solidi B* **1969**, *31*, 323.
(12) Wagner, J.; del Alamo, J. A. *J. Appl. Phys.* **1988**, *63*, 425.
(13) Haas, C. *Phys. Rev.* **1962**, *125*, 1965.
(14) Golikova, O. A.; Moizhes, B. Y.; Stilbans, L. S. *Sov. Phys. Solid State* **1962**, *3*, 2259.
(15) Veiland, L. J.; Kudman, I. *J. Phys. Chem. Solids* **1963**, *24*, 437.
(16) Hanna, M. C.; Lu, Z. H.; Majerfeld, A. *Appl. Phys. Lett.* **1991**, *58*, 164.
(17) Holmberg, H.; Lebedeva, N.; Novikov, S.; Kuivalainen, P.; Malfait, M.; Moshchalkov, V. V.; Kostamo, P. *IEEE Trans. Magn.* **2005**, *41*, 2736.

(18) Ma, T. Y.; Lee, S. C. *J. Mater. Sci.: Mater. Electron.* **2000**, *11*, 305.
(19) Wu, J.; Walukiewicz, W.; Li, S. X.; Armitage, R.; Ho, J. C.; Weber, E. R.; Haller, E. E.; Hai, L.; Schaff, W. J.; Barcz, A.; Jakiela, R. *Appl. Phys. Lett.* **2004**, *84*, 2805.
(20) Masumdar, E. U.; Gaikwad, V. B.; Pujari, V. B.; More, P. D.; Deshmukh, L. P. *Mater. Chem. Phys.* **2003**, *77*, 669.
(21) Harrison, R. J.; Houston, P. A. *J. Cryst. Growth* **1986**, *78*, 257.
(22) Yu, P. Y.; Cardona, M. *Fundamentals of Semiconductors: Physics and Materials Properties*; Springer-Verlag: Berlin, 1999.
(23) Nolte, D. D.; Walukiewicz, W.; Haller, E. E. *Phys. Rev. Lett.* **1987**, *59*, 501.
(24) Wang, D.; Chang, Y. L.; Wang, Q.; Cao, J.; Farmer, D. B.; Gordon, R. G.; Dai, H. *J. Am. Chem. Soc.* **2004**, *126*, 11602.
(25) Huang, Y.; Duan, X.; Cui, Y.; Lieber, C. M. *Nano Lett.* **2002**, *2*, 101.
(26) Bryllert, T.; Wernersson, L. E.; Froberg, L. E.; Samuelson, L. *IEEE Electron. Device Lett.* **2006**, *27*, 323.
(27) Yun, Y. S.; Park, J. Y.; Oh, H.; Kim, J. J.; Kim, S. S. *J. Mater. Res.* **2006**, *21*, 132.
(28) Cui, Y.; Duan, X.; Hu, J.; Lieber, C. M. *J. Phys. Chem. B* **2000**, *104*, 5213.

NL062886W